Engineering Structures 264 (2022) 114471

Contents lists available at ScienceDirect

Engineering Structures

journal homepage: www.elsevier.com/locate/engstruct

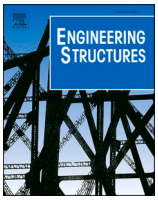

Behavior of flat slabs with partial use of high-performance fiber reinforced concrete under monotonic vertical loading

Brisid Isufi [a,*], João Pedro Relvas [a], Carla Marchão [a], António Pinho Ramos [a,b]

[a] NOVA School of Science and Technology, Caparica, Portugal
[b] CERIS, Lisbon, Portugal

ARTICLE INFO

Keywords:
High performance concrete
Fiber reinforced concrete
FRC
HPFRC punching shear
Flat slab

ABSTRACT

Reinforced concrete flat slabs are used worldwide in multi-story buildings. In these slabs, the design is often governed by punching shear and serviceability. The mitigation of these issues during design usually leads to increased raw material consumption and costs. Previous studies have shown that using Fiber Reinforced Concrete (FRC) or High-Strength Concrete (HSC) only at the vicinity of the column, while casting the rest of the slab with Normal Strength Concrete (NSC), can lead to an improved behavior under gravity loads in terms of both serviceability and ultimate capacity. Motivated by these results and the scarcity of previous tests, the present paper experimentally investigates the applicability of High-Performance Fiber Reinforced Concrete (HPFRC) as an alternative material that can be seen as an improvement over FRC and HSC, allowing a combination of ductility and strength. In addition, the HPFRC used in this paper is self-compacting, thus reducing the labor costs associated with concrete vibration. Five 150 mm thick flat slabs were tested under monotonically increasing punching load. The experimental variables were the flexural reinforcement ratio and the extent of the HPFRC zone. One of the specimens was cast only with NSC and served as a reference slab. Results show that the solution was effective for both flexural reinforcement ratios considered. Cracking load, maximum load, as well as the displacement capacity were increased significantly, even for a small extent of HPFRC (1.5 times the effective depth from the face of the column). Regarding the ultimate load capacity, it was observed an increase of 44% to 58% for the specimens with lower reinforcement ratio (0.64%) and between 15%–21% for the specimens with higher reinforcement ratio (0.96%). The results indicate that the use of HPFRC is a promising solution regarding both serviceability and ultimate limit state design of reinforced concrete flat slabs under gravity loading, with obvious advantages in material savings and labor costs.

1. Introduction

Punching shear failure is often the governing failure mode in flat slabs. Potential solutions to increase punching shear strength include the increase of slab's thickness (either across the entire floor or only in the vicinity of the column, in the form of a drop panel) and the provision of punching shear reinforcement. The former leads to an increase in the consumption of raw materials by the increase of the volume of concrete, but also indirectly due to the increased weight and mass of the building that leads to increased demands for the entire structure. The latter (provision of punching shear reinforcement) has been shown to be very effective in increasing punching shear strength of flat slabs, but it is often labor intensive, prone to execution errors, and sometimes leads to a congestion of reinforcement near the column that makes casting of concrete difficult. In addition to punching shear, serviceability design often governs the design of reinforced concrete flat slabs. It should be noted that in general, the provision of punching shear reinforcement cannot mitigate serviceability issues.

With the development of concrete technology and the advent of advanced concrete materials such as high strength concrete (HSC), fiber reinforced concrete (FRC) and high-performance concretes (HPC), new possibilities have arisen to minimize the aforementioned problems in flat slabs and reduce the overall consumption of materials and/or labor costs. Significant research on the use of advanced concrete materials to mitigate punching shear issues in flat slabs started in the 1980s' and early 1990s' with works from Swamy and Ali [1], Narayanan and Darwish [2] on FRC and Marzouk and Hussein [3] on HSC, although previous works on small scale specimens also exist. Early studies showed

* Corresponding author at: Departamento de Engenharia Civil, NOVA School of Science and Technology, Campus Universitário, 2829-516 Caparica, Portugal.
E-mail address: b.isufi@campus.fct.unl.pt (B. Isufi).

https://doi.org/10.1016/j.engstruct.2022.114471
Received 28 December 2021; Received in revised form 8 April 2022; Accepted 22 May 2022
Available online 1 June 2022

that the use of HSC and FRC has great potential to increase punching shear strength and the overall performance of flat slabs subjected to gravity loading.

One of the main conclusions of the detailed literature review on the application of HSC and FRC in flat slabs, that can be found in Isufi and Ramos [4], is that the combination of HSC with FRC into a high performance fiber reinforced concrete (HPFRC) has not been sufficiently explored in flat slabs under gravity loading, with knowledge gap still remaining in this field. Such a combination is potentially beneficial for flat slabs subjected to punching shear because the high strength of concrete can lead to an increased punching shear strength, whereas steel fibers can reduce and control internal cracking, both leading to an increase of punching shear capacity. Experimental studies that have investigated this possibility in the past include Chanthabouala et al. [5], in which a FRC with compressive strength above 80 MPa was used in 150 mm thick slabs tested under gravity loading, Ozden et al. [6] that tested 120 mm thick circular slabs with 1.5 m diameter and Qi et al. [7], that tested 60 mm specimens with partial use of a concrete with compressive strength about 150 MPa. More tests on small scale slabs (thickness below 100 mm) can also be found in the literature.

The present study investigates the behavior of large-scale composite slabs under punching shear with hybrid use of conventional normal strength concrete (NSC) and high-strength fiber reinforced concrete. Due to the specificities of the later, which are not only related to compressive strength but also to performance in general (including durability, tensile behavior, self-compacting properties), this material is called high performance fiber reinforced concrete (HPFRC) from here on. The HPFRC is used only in a localized area of the slab-column connection, being the rest of the slab cast with NSC, to take full advantage of HPFRC characteristics and to compensate for its relatively high cost. So the hybrid use of HPFRC in this research aims to optimize the quantity of improved concrete (i.e. HPFRC) used, in order to have a more sustainable and economic solution, and it is motivated by past research on HSC slabs [8,9], FRC slabs [1,10–12] and UHPFRC slabs [13].

2. Description of HPFRC

The HPFRC mixture used was specifically developed by Nunes et al. [14,15] for the present research. The mix design is summarized in Table 1, along with details about each constituent. Portland cement with a compressive strength of 42.5 MPa at 28 days (CEM I 42.5R) was used. Limestone powder and silica fume were added. A high-range water reducer (superplasticizer) was used to give the mix the desired level of fluidity. Fine and coarse aggregates with maximum aggregate size of 8 mm were used. Finally, two types of steel fibers were used, as depicted in Fig. 1. The fiber volume fraction was $V_f = 1\%$, with 0.5% corresponding to triple hooked-end long fibers and 0.5% corresponding to short straight fibers. The hybrid mixture (with two types of fibers) was chosen after an extensive experimental campaign described in [14], which compared several single, binary and ternary mixtures and showed that the binary mixture used in this study had the best performance (highest crack mouth opening displacement at maximum load in a wedge-splitting test and good self-compacting properties).

Table 1
Mix proportions of the HPFRC.

Material	Quantity (kg/m^3)
Cement	531.86
Limestone powder	203.72
Silica fume	53.19
Water	147.85
Superplasticizer	12.55
Fine aggregates	811.82
Coarse aggregates	721.43
Steel fibers (long)	39.25
Steel fibers (short)	39.25

Table 2 summarizes the main properties of the steel fibers, namely the length (L), diameter (d), aspect ratio L/d, the nominal tensile strength f_t as well as the modulus of elasticity E.

Detailed material characterization is provided in [14]. Based on [14], the HPFRC developed presents a compressive strength for 150-mm width cubes of about 125 MPa and for 150-mm diameter and 300-mm high cylinder of 114 MPa at 28 days. The flexural behavior is characterized by a stress at the limit of proportionality $f_L = 10$ MPa and residual flexural tensile strengths $f_{R1} = 15.4$ MPa (for crack mouth opening displacement – CMOD – in a three-point bending test of 0.5 mm), $f_{R2} = 18.0$ MPa (for CMOD = 1.5 mm), $f_{R3} = 16.4$ MPa (for CMOD = 2.5 mm) and $f_{R4} = 12.9$ MPa (for CMOD = 3.5 mm) [14]. It should be noted that f_L and f_{R1} to f_{R4} values are average values. Further details can be found in Nunes et al. [14]. Further details about the characterization of materials used to build the slab specimens presented in this paper are presented in Section 3.3.

3. Experimental program

3.1. Description of the specimens

Five specimens were produced and tested under monotonic punching loading. All specimens had a thickness of 150 mm, and an octagonal shape with overall dimensions of 2.2 m by 2.2 m (Fig. 2). The main experimental variables were the flexural reinforcement ratio (0.64% and 0.96%) and the size of the HPFRC zone (600 mm square and 960 mm square) that corresponded to an extent ranging from 1.5d to 3.0d from the face of the column, where d is the average effective depth of the top reinforcement. Two specimens with different sizes of the HPFRC zone were cast for each flexural reinforcement ratio. For the flexural reinforcement ratio of 0.64%, an additional reference specimen (without HPFRC) was cast. A corresponding reference specimen with the higher flexural reinforcement ratio (0.96%) was not produced, because a specimen with similar flexural reinforcement ratio already existed, tested in previous research (read further in Section 4.2). The specimens were named following this convention: “HP” (representing HPFRC) followed by the width of the HPFRC zone (in millimeters), followed by an underscore and the letter “R” (for reinforcement) followed by the flexural reinforcement ratio (as a percentage). For example, specimen HP960-R0.6 is a specimen with a 960 mm square region with HPFRC and flexural reinforcement ratio 0.64%. The geometry of the specimens is presented in Fig. 2.

Flexural reinforcement details are provided in Fig. 3. For all specimens, 12 mm and 10 mm deformed rebars were used for the top and bottom reinforcement meshes, respectively. As usually adopted in the detailing of flat slabs, the spacing of top rebars near the column (up to roughly 3 times the effective depth from the face of the column) was smaller compared to the outer region. Fig. 3 presents also the positioning of the strain gauges that were installed (further discussed in Section 3.2). Although the specified nominal concrete cover was 20 mm, the exact effective depth, d, of the top bars was measured right before casting and the results are shown in Table 3. In addition, Table 3 also presents the average top flexural reinforcement ratios ρ_l (calculated based on Eurocode 2 [16]) and the width of the HPFRC zone expressed in value and as a multiple of d from the face of the support (column).

The specimens were cast-in-place on a plywood panel formwork that was prepared near the testing facilities at Nova School of Science and Technology (Fig. 4). In order to cast the specimens with different concretes (conventional concrete and HPFRC), it was necessary to use a general-purpose fine galvanized steel mesh (diameter 0.5 mm and square shaped, with size 13 mm) at the interface between the two zones, connected to the top and bottom reinforcement bars Fig. 4-c. Considering the properties of HPFRC, namely its self-compacting properties as well as the relatively short setting time, it was decided to cast the outer region first (with conventional concrete) followed by the HPFRC soon

Fig. 1. Steel fibers used in HPFRC: a) Triple hooked-end hooked fibers with diameter 0.9 mm and length 60 mm; b) straight fibers with diameter 0.2 mm and length 13 mm (ruler divisions: cm and mm).

Table 2
Properties of the steel fibers.

No.	Figure	L (mm)	d (mm)	L/d	f_t (MPa)	E (GPa)
1	Fig. 1-a	60	0.9	65	2300	200
2	Fig. 1-b	13	0.2	65	2750	200

after (Fig. 4-a, b). After casting, the specimens were covered using a wet geotextile membrane and a plastic sheet for at least 7 days to prevent excessive water loss due to evaporation. As it is shown in the following sections of this paper, this casting procedure resulted appropriate.

3.2. Test setup and instrumentation

The specimens represent the hogging moment region near a column of an interior flat slab panel with equal spans in both orthogonal directions up to the zero moment line, supported on 250 mm square columns. The test setup is shown in Fig. 5. A central hydraulic jack with 1000 kN capacity and a maximum stroke of 153 mm was used to apply the load at a rate of approximately 150 N/s. The slab specimen was connected to the laboratory strong floor using a system of four spreader beams and eight strands as illustrated in Fig. 5.

To measure the applied load throughout the test, eight load cells were installed on top of the slab at the locations of the strands, along the perimeter of the specimen. Eleven displacement transducers were installed on top of the slab and five additional ones were installed on the bottom surface, as shown in Fig. 6. Pairs of strain gauges were installed in diametrically opposite sides of five reinforcement rebars for each specimen, in the positions shown in Fig. 3, corresponding to the bars of the top mesh with lower effective depth.

3.3. Materials

3.3.1. Characterization of the fresh state

To evaluate the flowing ability of the fresh mix in non-confined conditions the slump flow test was carried out, according to EN

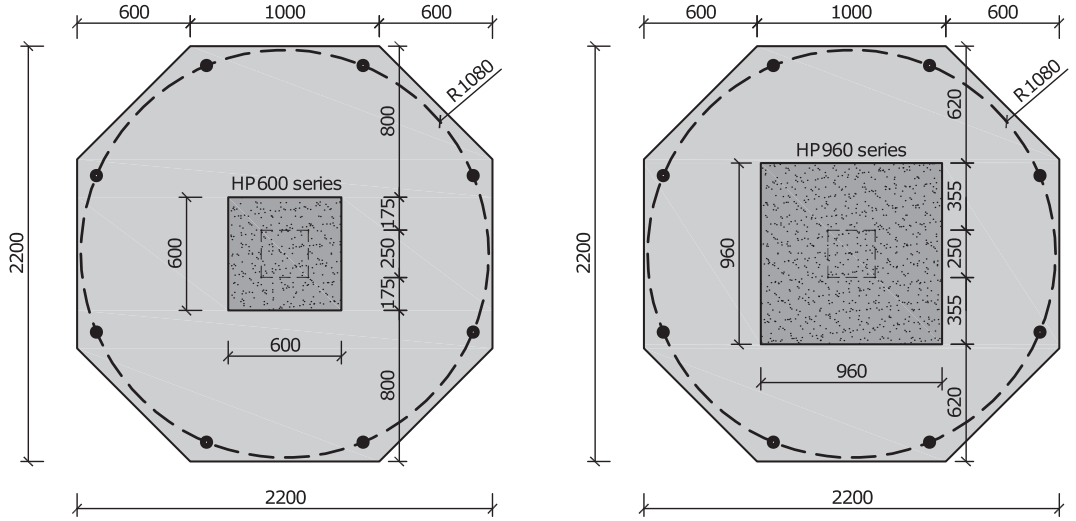

Fig. 2. Geometry of the specimens (dimensions in mm).

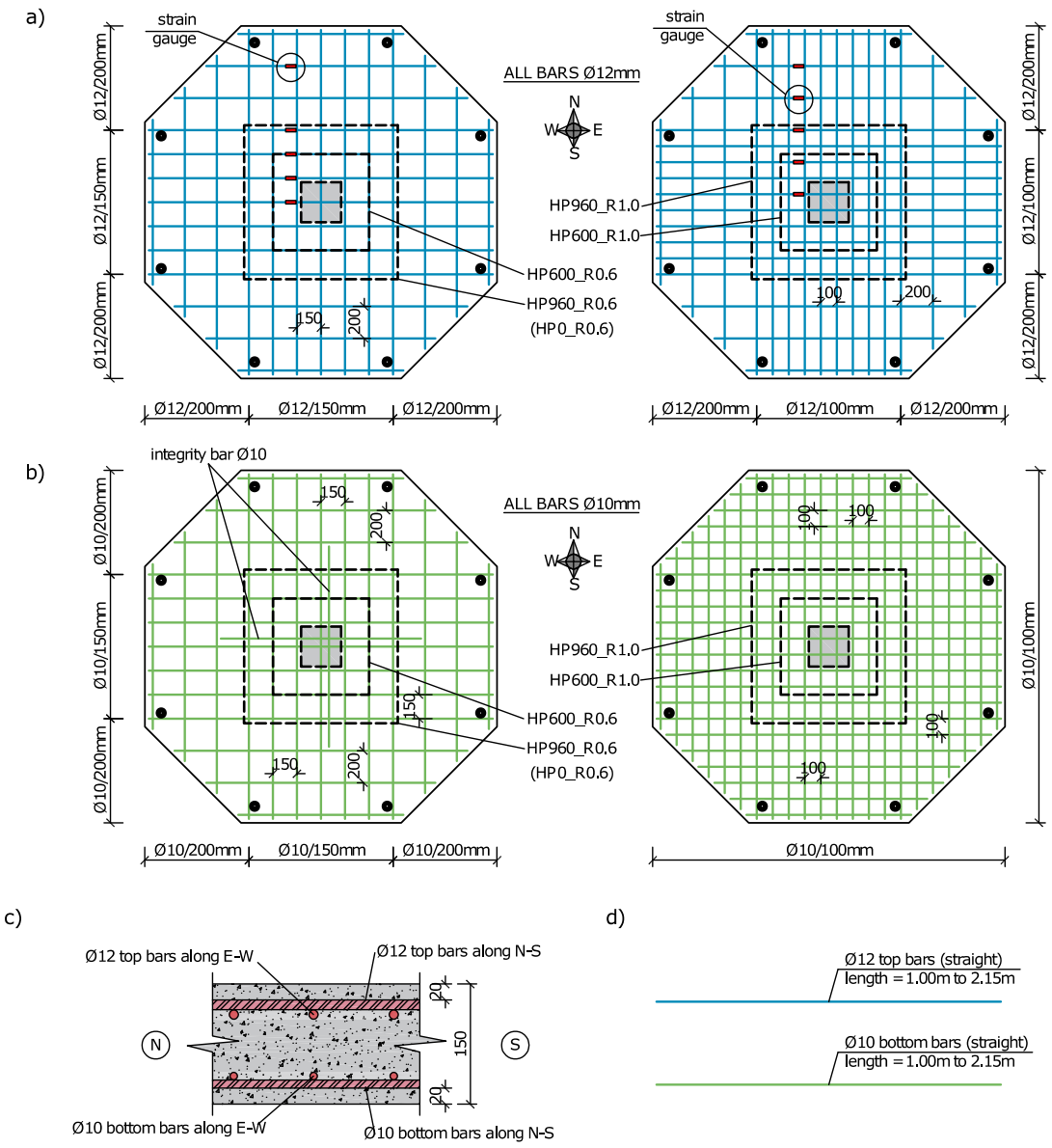

Fig. 3. Flexural reinforcement and strain gauges: a) top rebars; b) bottom rebars; c) cross-section detail; d) reinforcement detail.

Table 3
Characteristics of the specimens.

Specimen	d (mm)	ρ_l (%)	HPFRC width c_{hpfrc} (mm)	HPFRC extent (d)
HP0_R0.6	117.7	0.64	0	0d
HP600_R0.6	118.4	0.64	600	1.5d
HP960_R0.6	118.0	0.64	960	3.0d
HP600_R1.0	117.5	0.96	600	1.5d
HP960_R1.0	117.9	0.96	960	3.0d

12350-8 [17]. Test results are the slump-flow diameter (D_{flow}) and the time needed to reach the 500 mm diameter (t_{500}). Table 4 shows the results of the test in the fresh state for the indicated mixtures. The results are close to those obtained by Nunes et al. [14].

3.3.2. *Mechanical properties*

Standard cubes with 150 mm width (six cubes for specimen HP0_R0.6 and three for the remaining specimens) and three cylinders with 150 mm diameter and 300 mm height of conventional concrete were tested in compression for each slab specimen to determine the compressive strengths $f_{c,cube}$ and f_c respectively, according to EN 12390-3 [18]. Prior to crushing, the cylinders were used to measure the modulus of elasticity, E, according to EN 12390-13 [19]. The tensile splitting strength of conventional concrete, $f_{ct,sp}$ was obtained by tensile splitting tests of three cylinders for each slab, according to EN 12390-6 [20]. The concrete properties for each specimen, at the date of the tests, and the corresponding coefficient of variation (COV), are summarized in Table 5.

A detailed characterization of the developed HPFRC has been presented in earlier works [14,15], as mentioned in Section 2. To check compliance with previous tests, five 100 mm cubes, three 150 mm cubes and three standard cylinders were cast for each slab. The 100 mm cubes were used in specimens where the compressive resistance of 150 mm cubes exceeded the operational capacity of the testing machine. The concrete properties for each specimen and the corresponding coefficient of variation (COV) are summarized in Table 6. The tests were carried out on the same day as the corresponding slab.

The results from Table 6 indicate that similar compressive strengths were achieved compared to Nunes et al. [14], indicating that the mixing procedure was properly followed.

The steel reinforcement used for both layers of reinforcement

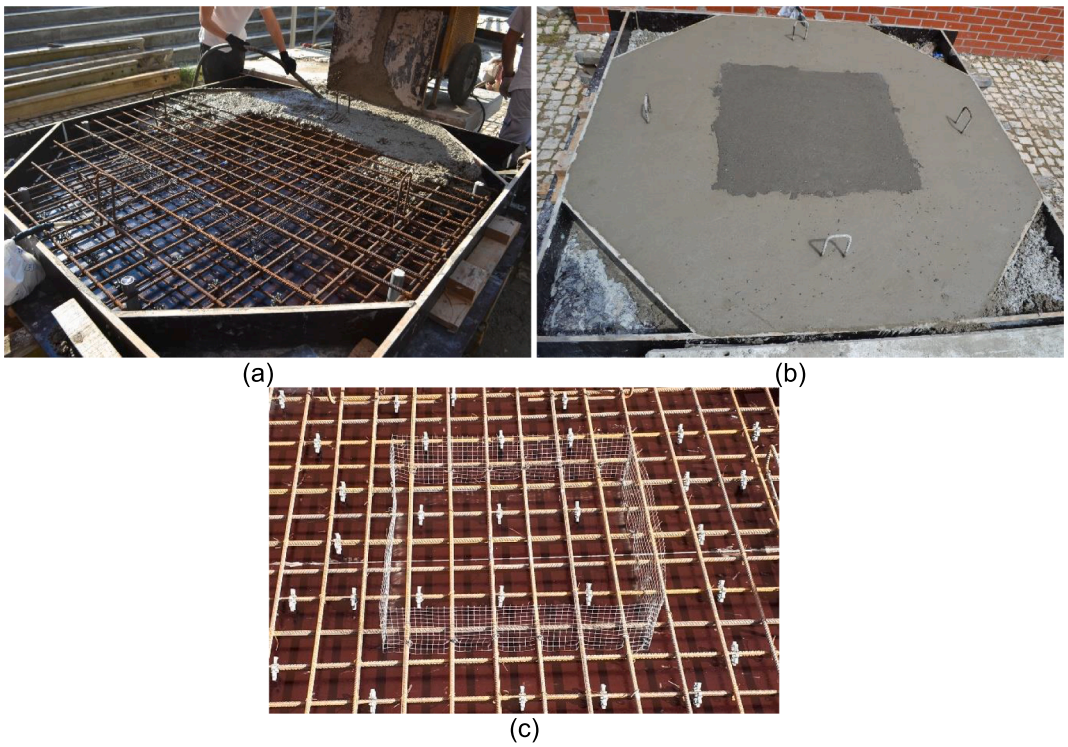

Fig. 4. Casting of specimens: a) formwork; b) finished product; c) steel net.

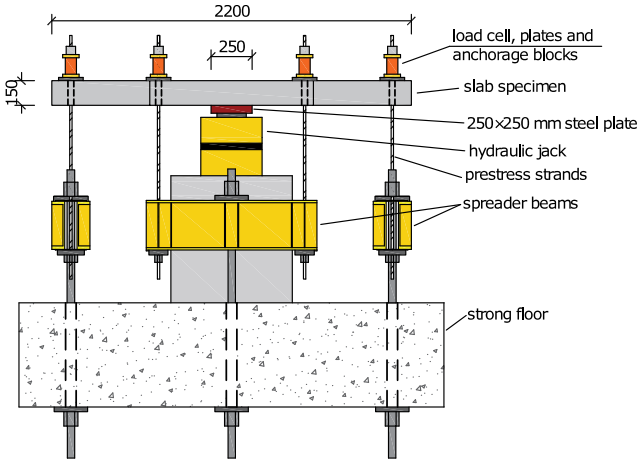

Fig. 5. Test setup.

consisted of deformed rebars. For the top bars, the yield strength was f_y = 547 MPa and the ultimate strength was f_u = 642 MPa.

4. Experimental results

4.1. Cracking and failure modes

The reference specimen (HP0_R0.6) showed a typical development of cracking throughout the test for flat slabs subjected to punching loads: radial flexural cracks appeared after the cracking load (about 70 kN) and grew steadily throughout the test. With the increase of the load, new cracks were formed on the top surface and the existing ones grew. The bottom surface suffered no noticeable damage until punching shear occurred, characterized by an intrusion of the steel plate support into the slab (refer to Fig. 7). On the top surface, a typical punching shear failure was noticed (Fig. 7-a). The saw-cut for this specimen shows a typical punching shear failure (Fig. 8).

For all the specimens with HPFRC, cracking was delayed compared to the reference specimen (HP0_R0.6). The cracking load, noticed by a change of slope on the load-displacement curve (Fig. 10), occurred for a vertical load around 115 kN for the specimens with a size of the HPFRC zone of 600 mm (HP600_R0.6 and HP600_R1.0), and around 130 kN for the other specimens with larger area of HPFRC (HP960_R0.6 and HP960_R1.0). Thus, increasing the area of HPFRC resulted in an increase of the cracking load, as expected. Also, the HPFRC specimens presented higher post-cracking stiffness than the reference specimen. Increasing the top longitudinal reinforcement ratio from 0.64% to 0.96% resulted in a slight increment on the post-cracking stiffness (comparing specimen HP600_R0.6 to HP600_R1.0 and specimen HP960_R0.6 to HP960_R1.0). The change of size of the HPFRC zone, for the specimens with the same top longitudinal reinforcement ratio, resulted in almost the same post-cracking stiffness (slope of the load – displacement curve after cracking almost parallel), although with a delayed beginning of the cracking phenomenon, that translated into smaller vertical displacements for the specimens with larger area of HPFRC.

After the appearance of the first crack in the HPFRC specimens, the development of the new cracks was visually similar to that of the reference specimen. Regarding cracks that were detected, some remained only within the HPFRC zone, others crossed the HPFRC central region and extended towards the edges of the specimen. As expected, the specimens with lower flexural reinforcement ratio presented more cracks for the same level of loading. For all specimens with HPFRC, the bottom surface did not suffer any visible damage until very close to failure.

In specimen HP600_R0.6, a shear failure outside the HPFRC zone started on one side of the HPFRC square zone. Due to likely redistribution of the load after the beginning of this failure, crushing of the bottom surface of the specimen occurred along NW – SE direction before propagation of the shear failure around the perimeter of the HPFRC region. The failure line on the bottom surface crossed even the HPFRC region, with a deviation caused by the presence of the support (see Fig. 7-b for HP600_R0.6). The saw-cuts presented in Fig. 8 and Fig. 9-a

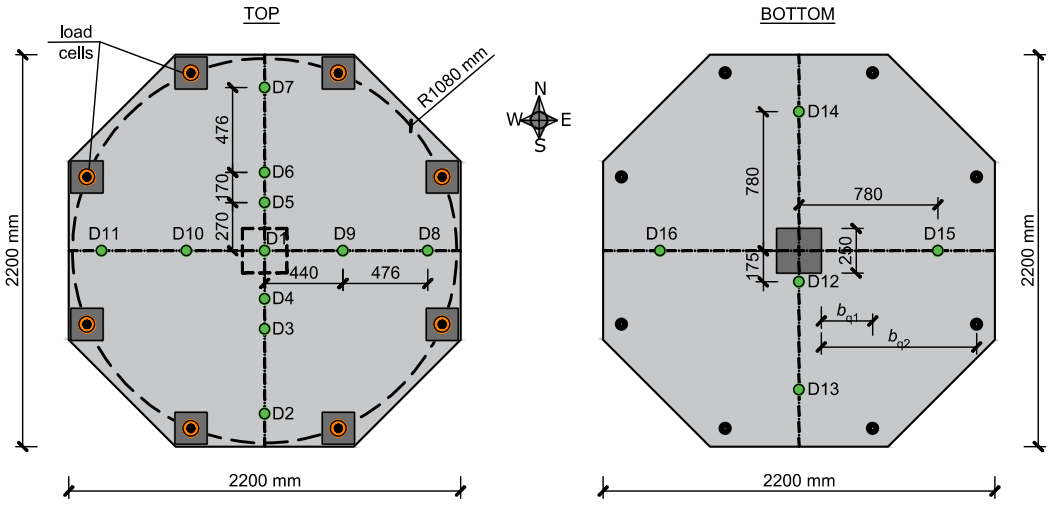

Fig. 6. Instrumentation: load cells and displacement transducers (units: mm).

Table 4
Slump flow test results.

Specimen	D_{flow} (mm)	t_{500} (s)
HP600_R0.6	680	13.1
HP960_R0.6	695	12.0

provide additional insight about failure of HP600_R0.6. Near the reinforcement bar on the north side, failure crossed the HPFRC zone, whereas at other angles, failure varied from shear failure outside the HPFRC zone to a combination of flexural damage and shear cracking.

Significant flexural cracks developed in HP960_R0.6 within the HPFRC region (Fig. 7-a) before failure. A premature punching shear failure occurred at one of the supports in the perimeter of the specimen at a load level that exceeded that of the similar specimen but with a smaller HPFRC region (HP600_R0.6). To understand whether this failure of HP960_R0.6 significantly affects the discussions in this paper, the specimen was cut in half, after the test, to investigate internal cracking. The saw-cut of Fig. 8 shows that there was a significant shear crack on the north side within the HPFRC zone, indicating that the specimen was close to failure. The crack was effectively controlled by the steel fibers, whereas cracking outside the HPFRC zone weakened the support region and likely caused failure at the border of the specimen.

In the two specimens with higher flexural reinforcement ratio (HP600_R1.0 and HP960_R1.0), shear failure occurred outside the HPFRC region. In the specimen with smaller width of the HPFRC region, failure affected three sides of the outer perimeter of the HPFRC zone. Delamination of the concrete cover is visible on the top surface, on three sides of the perimeter, in similarity with a typical punching shear failure with a large perimeter (Fig. 7). The failure perimeter was not closed (failure extended on three sides of the column when the test was stopped). In contrast to HP600_R0.6, the saw-cut (Fig. 8) shows that failure within HPFRC was not detected in HP600_R1.0.

In HP960_R1.0, the redistribution capacity of the shear force along the perimeter outside the HPFRC zone was even more limited due to the large perimeter of the HPFRC zone. This led to a shear failure resembling one-way shear in this specimen. However, the saw-cut (Fig. 8) along the N-S direction (the direction along which the bars had higher effective depth) shows that a shear crack had developed also on the south side, opposite to the side in which visible failure occurred, that led to the conclusion of the test. To investigate whether the shear crack was developed in the perpendicular direction, an additional cut was made (see Fig. 9-b). The additional cut showed that no significant shear cracking was present in the E-W direction.

In addition, the saw-cuts presented in Fig. 8 and Fig. 9 show that the solution used for the interface between the HPFRC and the NSC was

Table 5
Conventional concrete mechanical properties.

Specimen	$f_{c,cube150}$		f_c (MPa)		$f_{ct,sp}$ (MPa)		E (GPa)	
	(MPa)	COV	(MPa)	COV	(MPa)	COV	(GPa)	COV
HP0_R0.6	25.4	8.3%	24.4	1.9%	2.2	10.5%	29.0	5.3%
HP600_R0.6	25.2	2.8%	27.5	3.8%	2.2	20.7%	29.5	3.7%
HP960_R0.6	30.1	3.5%	26.0	2.2%	2.5	5.0%	27.5	4.8%
HP600_R1.0	28.1	5.5%	24.6	3.3%	2.2	22.1%	25.1	4.5%
HP960_R1.0	23.8	4.4%	25.5	5.1%	2.3	17.4%	25.6	4.7%

Table 6
HPFRC mechanical properties.

Specimen	$f_{c,cube150}$		$f_{c,cube100}$		f_c		E	
	(MPa)	COV	(MPa)	COV	(MPa)	COV	(GPa)	COV
HP600_R0.6	120.0	2.8%	N/A	–	126.1	0.8%	51.5	1.0%
HP960_R0.6	129.5	1.0%	130.1	0.3%	127.7	1.3%	49.7	1.7%
HP600_R1.0	N/A	–	126.6	3.4%	123.9	2.7%	49.3	2.7%
HP960_R1.0	N/A	–	124.0	5.1%	118.1	2.8%	N/A	–

*not applicable, or not available.

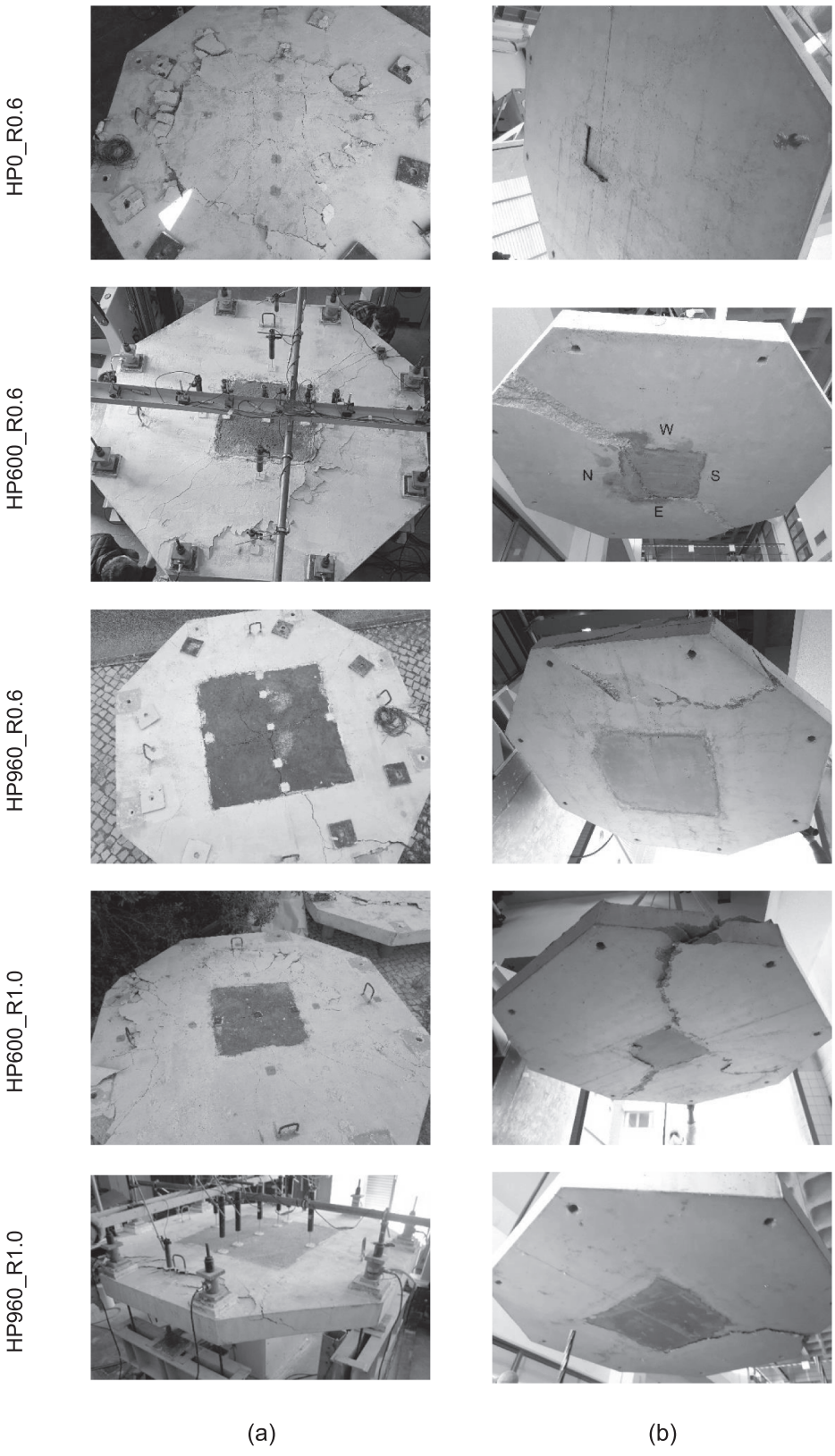

Fig. 7. Specimens after failure: a) top surface; b) bottom surface.

efficient, showing a good bond behavior between the two different concretes. Minor imperfections occurred at the bottom part of the HPFRC zone in some specimens due to the vibration of NSC which led to some intrusion into the zone that was supposed to be cast with HPFRC.

4.2. Load – Displacement relationships

The load (V) – displacement (u) curves for all specimens are presented in Fig. 10. The displacement u is obtained as the relative reading between the central displacement transducer on top of the slab (D1, see

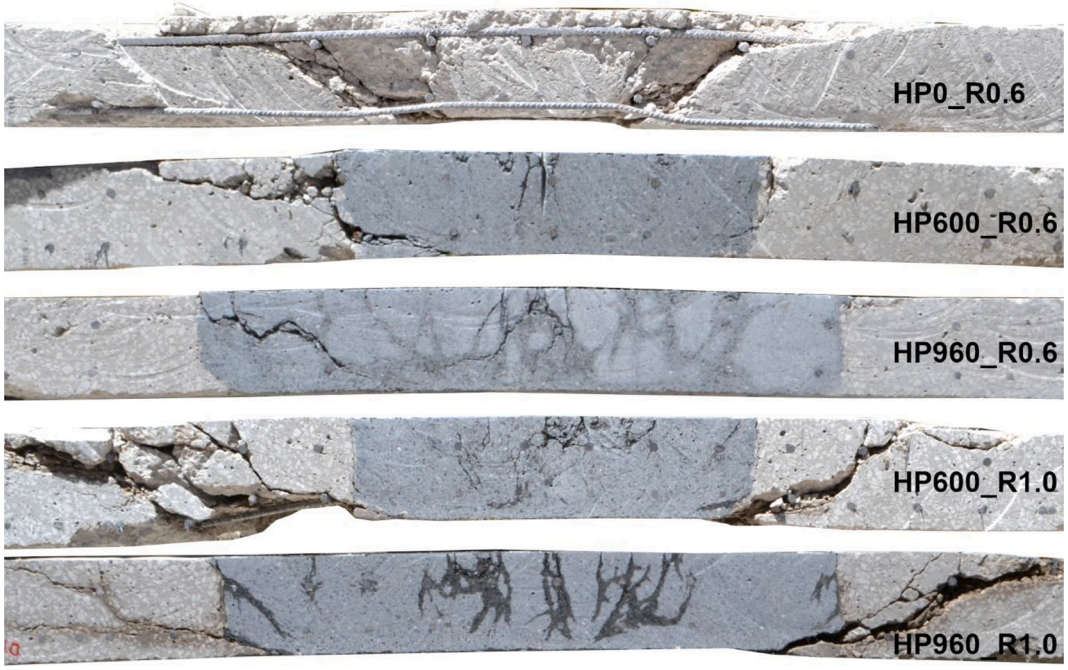

Fig. 8. Saw-cuts of the specimens along N-S direction.

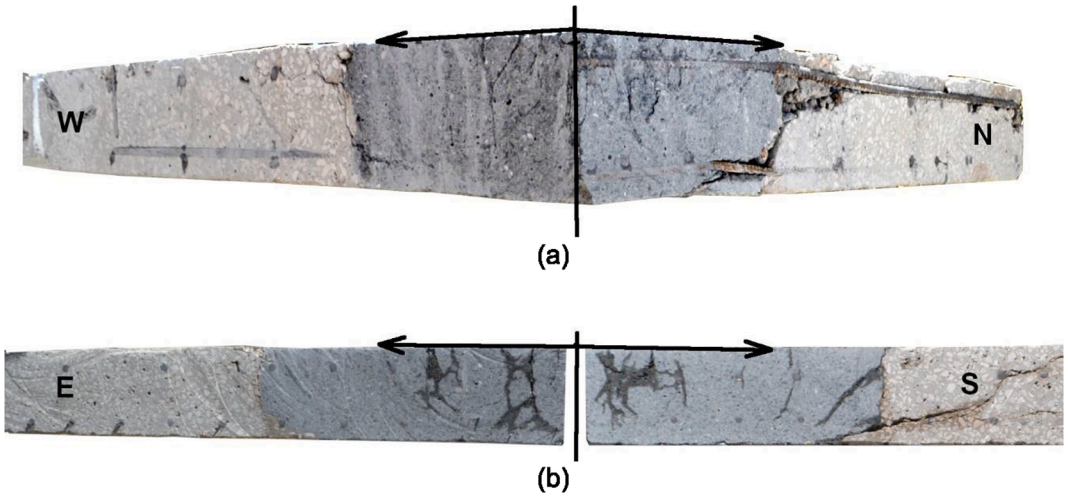

Fig. 9. Saw-cuts in two directions: a) specimen HP600_R0.6; b) specimen HP960_R1.0.

Fig. 6) and the average reading of the farthest displacement transducers from the center (D2, D7, D8 and D11, see Fig. 6). The load V was obtained as the sum of measurements from the eight load cells on top of the slab, plus the self-weight of the specimen and the contributing test setup components. In Fig. 10, the curves start at a load level equal to the self-weight, which was estimated to be approximately 21.5 kN for HP0_R0.6, and slightly greater for the other specimens (21.6, 21.7, 21.7 and 21.8 for HP600_R0.6, HP960, R0.6, HP600_R1.0 and HP960_R1.0, respectively). The small differences are due to the increased unit weight of HPFRC and due to the addition of eight steel plates under the load cells in the last two specimens (added to prevent failures at the border of the specimens). In specimen HP600_R1.0, it was necessary to perform an unforeseen unloading and reloading cycle due to a technical issue. In Fig. 10 and Fig. 11 the unloading branch is not presented for clarity reasons. The full load – displacement graph for this specimen is shown in Fig. 16 and discussed in Section 4.6.

Table 7 summarizes the main results, including maximum loads V_{exp},

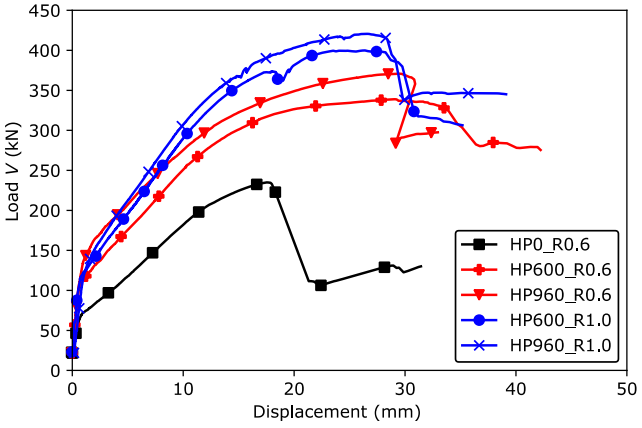

Fig. 10. Load – displacement relationships.

and displacements u_{max} corresponding to V_{exp}. Fig. 10 and Table 7 show that the role of HPFRC was fourfold in the specimens with the lowest flexural reinforcement ratio (R0.6 specimens): it increased the cracking load, the post-cracking stiffness, the ultimate load capacity of the specimens as well as the ultimate displacement. Referring to the specimens with flexural reinforcement ratio of 0.64%, the load capacity was increased by 44% for a 600 mm HPFRC zone width and approximately 58% for the other specimen (HP960_R0.6) with a larger HPFRC zone. The significant post-cracking stiffness means that the application of HPFRC can also be beneficial in mitigating serviceability issues in flat slabs.

To check whether the aforementioned observations hold true for the specimens with higher flexural reinforcement ratio (specimens with suffix R1.0), reference is made to a previously published specimen, named F0_R1.0 from Gouveia et al. [10]. Specimen F0_R1.0 was nominally identical to specimens HP600_R1.0 and HP960_R1.0, except that it was made entirely of conventional concrete with a compressive strength of 66.3 MPa. The effective depth of F0_R1.0 measured before casting was 117.5 mm [10]. Fig. 11 compares each set of HPFRC specimens with their respective reference specimen with conventional concrete.

Fig. 11 confirms that the effects of HPFRC hold true across different flexural reinforcement ratios. Comparing the two sets of specimens, it is noticed that the differences between the reference specimen and HPFRC specimens are superior in specimens with lower flexural reinforcement ratio. For the specimens with higher reinforcement ratio, the differences in load capacity between the reference slab and the slabs with HPFRC are lower, also because F0_R1.0 (reference specimen) had a relatively high compressive strength for the conventional concrete (66.3 MPa, as mentioned earlier). In this case, the capacity of the specimens with HPFRC was increased by 15% and 21% (HP600_R1.0 and HP960_R1.0 respectively).

Referring to specimens with HPFRC with different sizes of the HPFRC zone, it is noticed that the specimens with larger HPFRC zone had a higher load capacity. However, the increase in capacity was small: approximately 9% in specimens R0.6 and approximately 5% in R1.0 specimens. A likely explanation of this result is the fact that flexural yielding occurred in the vicinity of the column (as indicated by the significant reduction of tangent stiffness in Fig. 11 and as it will be proved later in this paper in Section 4.5). Also, especially in the specimens with larger area of HPFRC, flexural yielding weakened the corners of the specimens and some interaction with the test setup might have contributed to this result.

4.3. Evolution of deflections

Deflection profiles are presented in Fig. 12 for the reference specimen HP0_R0.6 based on readings from displacement transducers on top of the slab along two principal directions (see Fig. 6). In the N-S direction, readings from one displacement transducer are missing due to a technical issue. The deflections are calculated as the relative displacements measured by the central and the other displacement transducers. The profiles are shown for load increments of 50 kN and for the maximum load.

Comparing the deflection profiles along the two principal directions, it is observed that the behavior of the reference slab was fairly axisymmetric, with comparable deflections along the two directions. Deflections in the E-W direction (weak direction, with lower effective depth of the flexural reinforcement) were marginally larger.

The deflection profiles for the specimens with HPFRC are shown in Fig. 13. Similarly to HP0_R0.6, deflection profiles along the two principal directions were comparable, and only deflection profiles in the N-S direction (strong direction, with higher effective depth of the reinforcement bars) are shown in the figure. Comparing graphs corresponding to the same flexural reinforcement layout (i.e. specimens HP600_R0.6 and HP960_R0.6 from Fig. 13 and HP0_R0.6 from Fig. 12), it is noticed that the introduction of a HPFRC zone in the vicinity of the column resulted in smaller deflections for a given shear force. As expected, the deflections are smaller when the region with HPFRC is larger (i.e. in specimen HP960_R0.6). For a 200 kN shear force, the maximum deflection in HP0_R0.6 was 1.7 times higher than that in HP600_R0.6 and 2.5 times higher than that in HP960_R0.6. These results show that HPFRC can be effective in mitigating serviceability issues in flat slabs.

Referring to specimens with higher flexural reinforcement ratio in Fig. 13 (HP600_R1.0 and HP960_R1.0), the deflections for any given shear force are reduced even further compared to the specimens with lower flexural reinforcement, as expected. However, in this case the differences between the two specimens at loads below failure were small.

Table 7
Main results (maximum load and displacement, and failure mode).

Specimen	V_{exp} (kN)	u_{max} (mm)	Failure mode
HP0_R0.6	235.0	17.6	Punching shear
HP600_R0.6	338.9	29.0	Combination of shear outside HPFRC, shear inside HPFRC and flexure
HP960_R0.6	370.9	29.2	Shear inside HPFRC (ultimately limited by punching shear at a corner of the specimen)
HP600_R1.0	399.9	26.4	Punching shear outside HPFRC zone
HP960_R1.0	420.1	26.5	One-way shear outside HFRC zone

4.4. Changes in thickness

The change of thickness of a slab is an indicator of internal cracking. An approximate estimation of thickness change during the test can be obtained through readings of displacement transducers on top of the slab and D12 underneath the slab (see Fig. 6). To account for the fact that no displacement transducer is located on top of the slab at the exact location of D12, an approximate estimation was made based on readings from displacement transducers D1, D3 and D4 fitted into a second-degree polynomial. The approximate thickness change is then

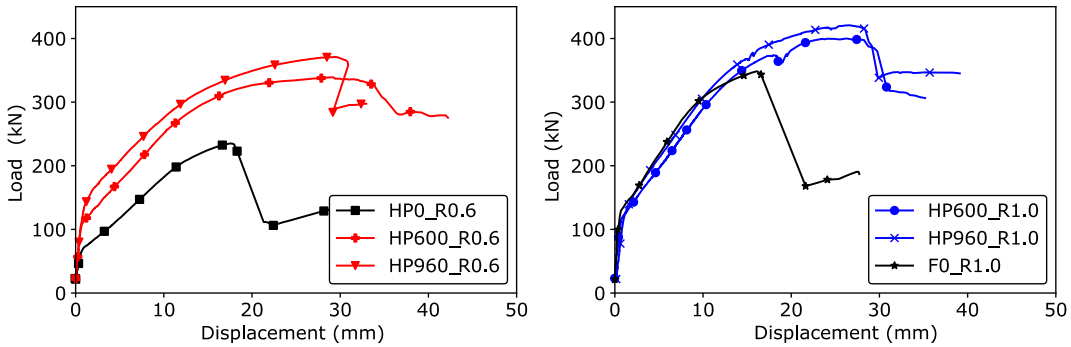

Fig. 11. Comparison of the load-displacement relationships with reference specimens without HPFRC.

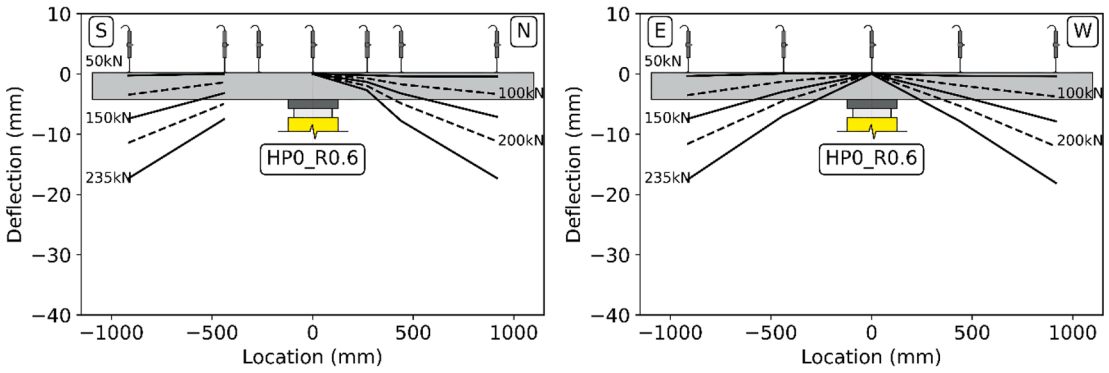

Fig. 12. Deflections of the reference specimen HP0_R0.6.

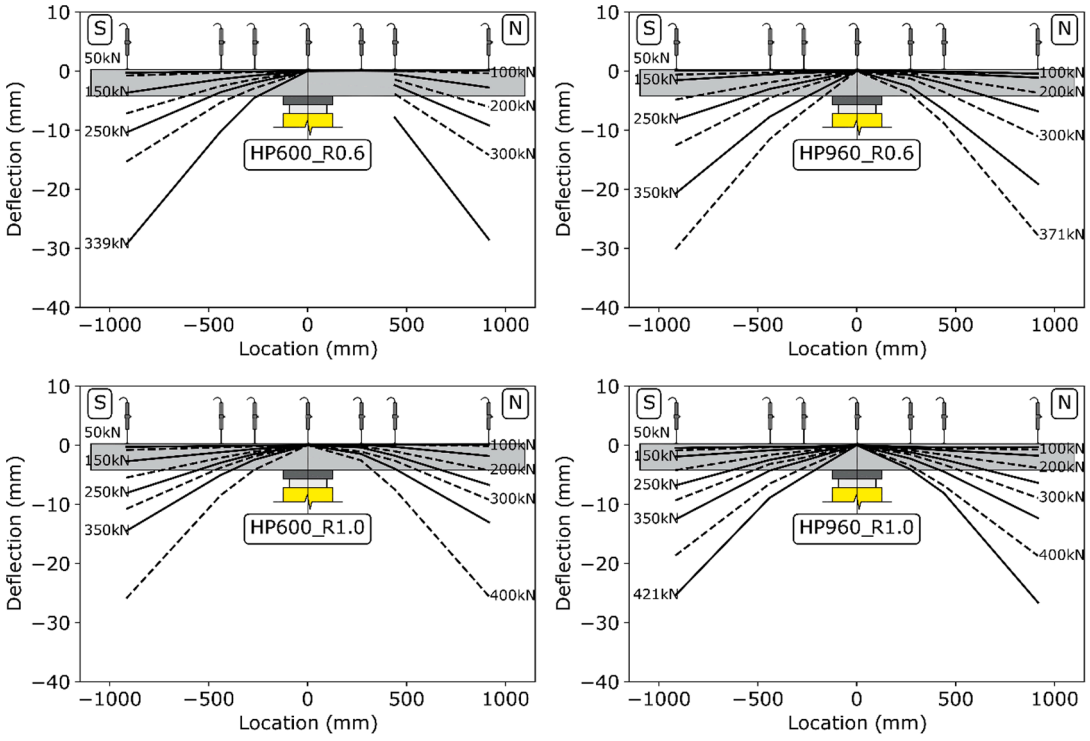

Fig. 13. Deflection profiles in N-S direction for specimens with HPFRC.

estimated as the difference between the reading on top of the slab and that of the bottom face.

The results are shown in Fig. 14 for all specimens. The figure shows that all the specimens had an increase of thickness under almost constant shear force after attaining the maximum shear force, indicating the presence of internal shear cracking in the vicinity of the central support region. Referring to HP960_R0.6, it can be seen that the tangent to the curve in Fig. 14 was approaching zero when failure at the corner of the specimen occurred (marked by the sudden drop of the load), indicating that the shear crack shown in Fig. 8 was growing and failure in the vicinity of the column was imminent, as hypothesized earlier.

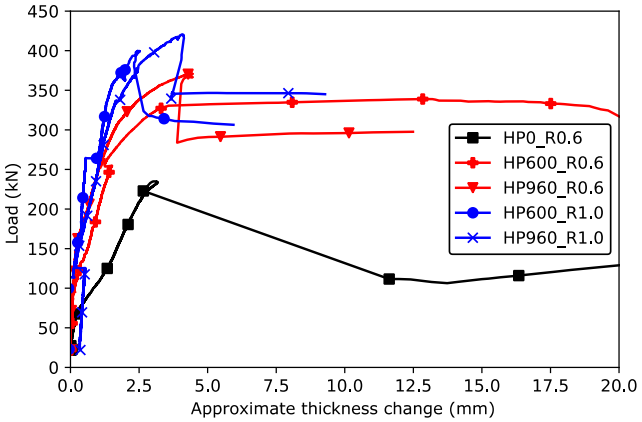

Fig. 14. Approximate changes in thickness.

4.5. *Flexural reinforcement strains*

Strains measured by strain gauges installed in the top flexural reinforcement mesh (see Fig. 3) are presented in Fig. 15 for various load levels, including the maximum load. The strains were small up to load levels corresponding to a linear elastic behavior of the specimens (see Fig. 10). With the increase of the applied load, strains progressively

increased. For the reference specimen HP0_R0.6, Fig. 15 indicates that strains decreased along the radius of the slab for all load levels. The introduction of a HPFRC zone near the column seems to influence the distribution of strains along the radius: for the same load level the strains were higher on the reference specimen when compared with the specimens that used HPFRC, showing the contribution of the steel fibers on the flexural behavior.

An important observation from Fig. 15 is that failure did not occur at the level of global flexural yielding of the specimen, for any of the specimens (i.e., not all instrumented bars had yielded when the maximum load was attained). For all specimens, strain was below, albeit close to, yielding at the instrumented bar farthest from the center of the slab. Comparing strain profiles for the same level of loading in Fig. 15, it is observed that, as expected, strains are generally higher in specimens with lower flexural reinforcement ratio.

4.6. Effect of unloading and reloading

In specimen HP600_R1.0, it was necessary to perform an unexpected unloading and reloading cycle due to a technical issue, as already mentioned before. The full load – displacement graph for this specimen is shown in Fig. 16. Note that, for clarity, this unloading - reloading cycle was omitted in Fig. 10 where the force – displacement relationships are presented for all the tested specimens.

According to Koppitz et al. [21], unloading – reloading cycles normally have a small effect on the punching shear resistance of flat slabs. The effects become more pronounced in the case of strengthening after unloading and in the case of thin and lightly reinforced slabs, which is not the case of HP600_R1.0. Although an exact evaluation of the effect of

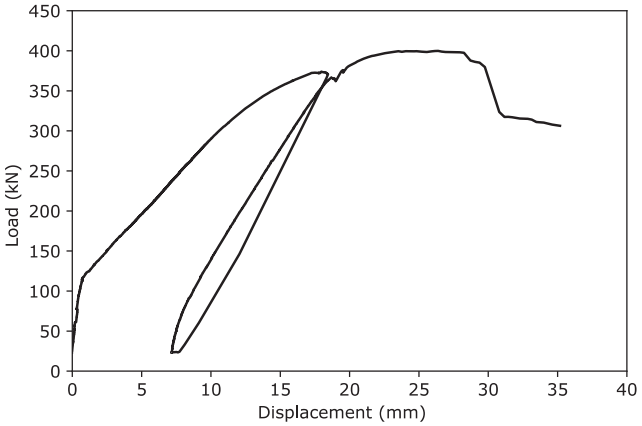

Fig. 16. Full load – deflection curve of specimen HP600_R1.0, including the unloading – reloading cycle.

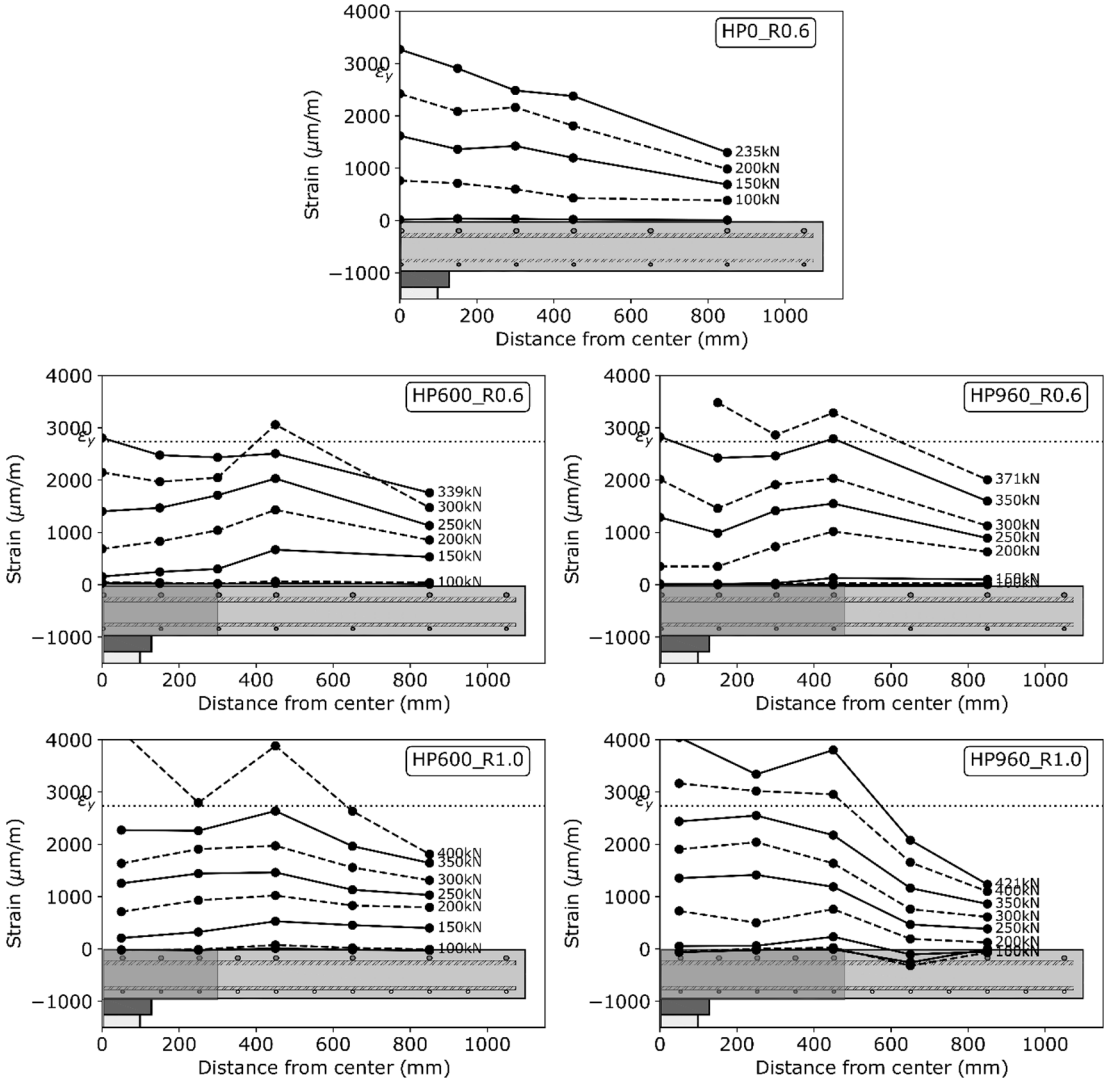

Fig. 15. Evolution of strains in top flexural reinforcement.

this unloading – reloading cycle is not possible with the available experimental data presented in this study, it is important to note firstly that failure of HP600_R1.0 occurred while the specimen had a small tangent stiffness, almost zero (see Fig. 16), indicating that a further significant increase of the shear force capacity was not expected. Strain gauge readings (see Section 4.5) confirm that specimen HP600_R1.0 was experiencing significant yielding before failure (although not all rebars along the entire width have yielded). Secondly, the specimen was able to recover the load it was carrying before unloading and further increased it. Finally, Fig. 16 shows that the unloading and reloading cycle was narrow, with almost linear unloading and reloading behavior. For these reasons, the effect of this unloading – reloading cycle is expected to be small on the interpretation of the results presented in this paper.

5. Capacity assessment

Throughout the years, several punching shear capacity prediction models have been developed for FRC [2,22,23]. Although these studies do not specifically address HPFRC, recent studies have shown that modifications can be made to make them suitable for materials with higher strength. For example, de Sousa et al. [24] studied the possibility of applying a model based on the Critical Shear Crack Theory (CSCT [25]) for slabs with rational use of UHPFRC.

The punching capacity of the specimens presented in this paper was estimated based on CSCT with modifications and simplifications as explained below, based on previous works from [10,22,24]. According to CSCT, the punching capacity is estimated at the intersection of a load – rotation relationship curve with an appropriate failure criterion. To estimate the load – rotation curve, the following expression (1) based on Model Code 2010 [26] (Level III of approximation) was used:

$$\psi = 1.2\frac{r_s}{d}\frac{f_y}{E_s}\left(\frac{V}{V_{flex}}\right)^{3/2} \tag{1}$$

where ψ is the slab's rotation, r_s is the radius of the slab, d is the average effective depth, f_y is the steel yield strength, E_s is the modulus of elasticity of steel, V is the shear force and V_{flex} is the flexural capacity, which for the specimens presented herein can be estimated using equation (2) [10]:

$$V_{flex} \approx 8\frac{B}{2\left(b_{q1}+b_{q2}\right)}m_R \tag{2}$$

where $B = 2.2$ m is the width of the specimen (Fig. 2), b_{q1} and b_{q2} are the projected distances from the face of the column to the load cells (see Fig. 6). The quantity m_R represents the nominal moment capacity per unit width of the slab. For hybrid slabs with partial use of HPFRC, m_R can be estimated by equation (3) (based on [10]):

$$m_R = \frac{m_{R,hpfrc}c_{hpfrc} + m_{R,NC}\left(B - c_{hpfrc}\right)}{B} \tag{3}$$

where c_{hpfrc} is the width of the zone with HPFRC (Table 3) and $m_{R,NC}$ is the moment capacity of the part of the slab with conventional concrete. To calculate the moment capacity $m_{R,hpfrc}$ of HPFRC, the following expression (4) based on Maya et al. [22] was used:

$$m_{R,hpfrc} = f_y\rho d^2\left[1-\frac{\beta_1}{2}\left(\frac{f_y\rho + f_{ct2,f}h/d}{\alpha_{cc}f_c + f_{fct2,f}}\right)\right] + \frac{f_{ct2,f}}{2}h^2\left[1-\left(\frac{f_y d\rho/h + f_{fct2,f}}{\alpha_{cc}f_c + f_{ct2,f}}\right)\right] \times \left[1+\left(\frac{f_y d\rho/h + f_{ct2,f}}{\alpha_{cc}f_c + f_{ct2,f}}\right)(1-\beta_1)\right] \tag{4}$$

with $\alpha_{cc} = 1$ and $\beta_1 = 0.8\text{-}(f_c\text{-}50)/400$. The tensile stress for a crack opening of 3 mm is denoted as $f_{ct2,f}$ in Eq. (4). For the HPFRC used in this study, $f_{ct2,f}$ was assessed based on an inverse analysis based on three point bending tests (read more in [27]). The flexural reinforcement ratio ρ is calculated based on the width of the HPFRC zone based on Fig. 3. The quantities f_y, f_c and h in Eq. (4) represent the steel yield strength, HPFRC compressive strength and slab thickness equal to 150 mm, respectively.

The failure criterion, for failure within the HPFRC zone, is based on Maya et al. [22], according to which the capacity (V_R) can be obtained using equation (5):

$$V_R = V_{R,c} + V_{R,f} \tag{5}$$

where $V_{R,c}$ is the contribution of concrete and $V_{R,f}$ is the contribution of fibers. The contribution of concrete can be estimated from [25], as follows:

$$V_{R,c} = \frac{3}{4}\frac{\sqrt{f_c}}{1+15\frac{\psi d}{d_{g0}+d_g}}b_0 d \tag{6}$$

where b_0 is the control perimeter located at a distance $0.5d$ from the face of the column, d_g is the maximum aggregate size and d_{g0} is a reference aggregate size equal to 16 mm. The aggregate size is taken equal to zero because the concrete is high-strength. The contribution of fibers can be expressed as follows (equation (7)) [22]:

$$V_{R,f} = A_p\sigma_{t,f} \tag{7}$$

where A_p is the area of the horizontal projection of the critical shear crack around the column and $\sigma_{t,f}$ is the fiber bridging stress (a detailed explanation can be found elsewhere [22,24,27]), as a function of the opening of the shear crack.

For failure outside the HPFRC zone, the failure criterion is based on the CSCT as described in [25] but with an adequate control perimeter taken at a distance $0.5d$ from the HPFRC zone.

The results are presented in Fig. 17 for all the specimens. The prediction of CSCT is quite close to the experimental results for all the specimens. For the specimens with HPFRC, the results are consistent with what was observed during the experiments. Firstly, failure occurred for a load close to the flexural capacity (refer to Section 4.5). Secondly, Fig. 17 predicts that failure outside the HPFRC zone is the most critical one for the specimens under consideration, except for specimen HP960_R1.0, in which it appears that both failure modes (outside and inside the HPFRC zone) were close to each-other. The figure also shows that a punching shear failure was quite difficult to be reached for the tested flexural reinforcement ratios (because flexural yielding takes precedence, in contrast to the reference specimen HP0_R0.6), which demonstrates the potential of HPFRC in avoiding punching shear failures for flexural reinforcement ratios commonly used in practice. A complete failure surface within the HPFRC zone was not developed in any of the specimens, so the ultimate capacity of slab with HPFRC governed by punching shear cannot be assessed by the present experimental work.

6. Conclusions

Five monotonic concentric punching tests were performed on flat slab specimens with varying flexural reinforcement ratio and varying extent of the zone with HPFRC in the vicinity of the column. The tests experimentally explored the possibility of enhancing the performance of composite conventional concrete – HPFRC large scale flat slab specimens. The following main conclusions resulted from this study:

1. HPFRC with compressive strength around 125 MPa and 1% fiber volume fraction (hybrid mixture of 0.5% corresponding to triple hooked-end long fibers and 0.5% corresponding to short straight fibers) applied over at least $1.5d$ from the face of the column was sufficient to significantly increase the capacity of the specimens (around 44% for specimen HP600_R0.6 compared to the reference specimen HP600_R0).

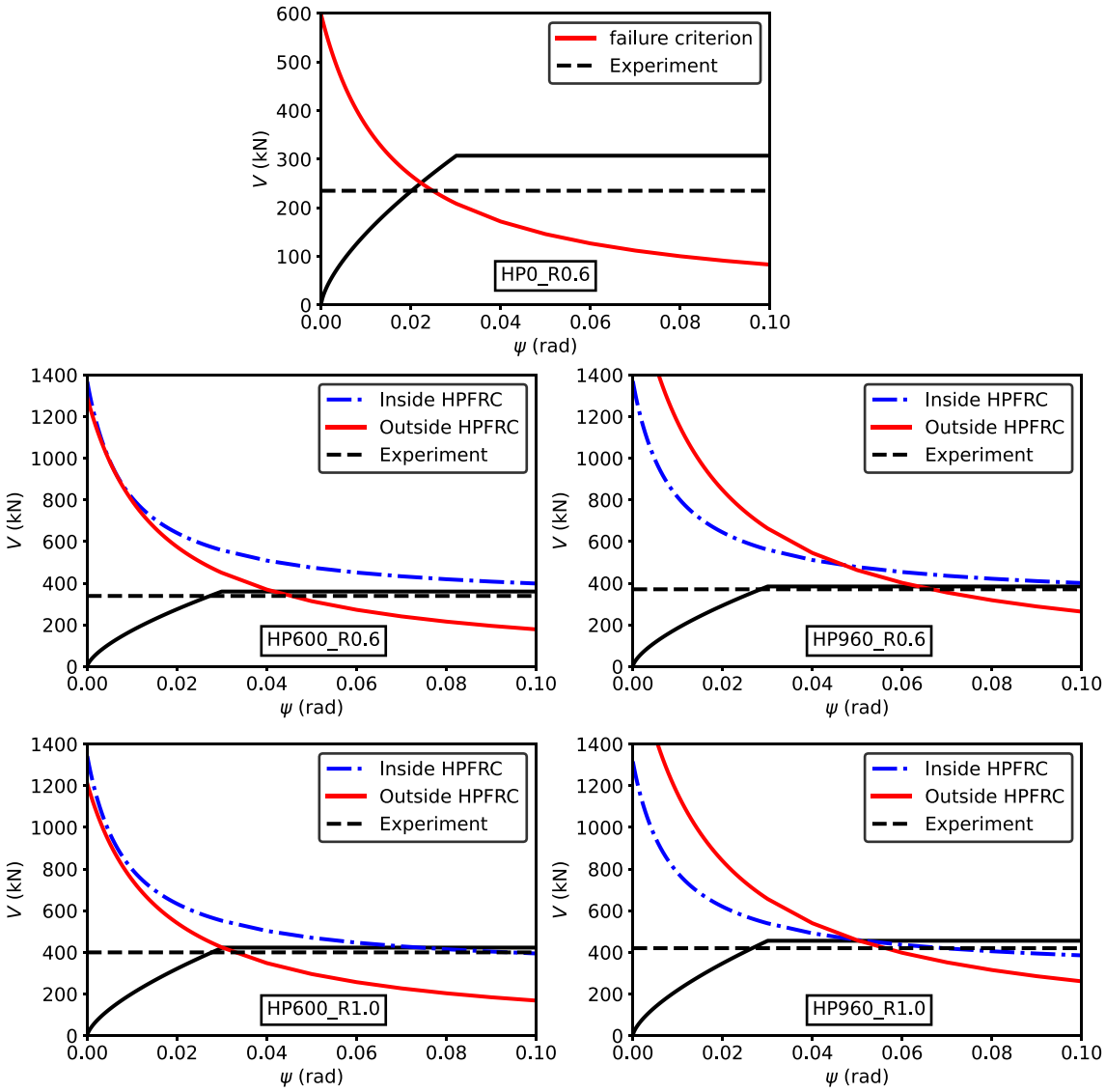

Fig. 17. Capacity assessment based on Critical Shear Crack Theory.

2. The use of HPFRC resulted successful in increasing the load capacity for both flexural reinforcement ratios considered in this research. For a longitudinal reinforcement ratio of 0.64% the load capacity was increased 44–58%. The increment of load capacity was 15–21% for the slabs with a longitudinal reinforcement ratio of 0.96%.
3. The use of HPFRC changed the failure mode of the specimens by pushing failure out of the HPFRC zone for the specimens with higher flexural reinforcement ratio. For lower flexural reinforcement ratio, HPFRC was able to reduce the brittleness of the shear failure, by effectively controlling the shear crack and thereby postponing failure.
4. Besides increasing the load capacity, HPFRC delayed initial cracking of the specimens. The solution used in this paper is therefore beneficial for the Serviceability Limit State design of flat slabs, even though HPFRC was applied over only a limited region near the column support.
5. Comparing specimens with the same flexural reinforcement ratio but with different sizes of the HPFRC zone, the capacity increase was rather limited, in the range of 5% to 10% with HPFRC extending from 1.5d to 3.0d from the face of the column (meaning 2.56 times increase of HPFRC material consumption), resulting in a low cost-benefit. The rather small capacity increase was likely the result of flexural yielding as well as some interference of the test setup due to cracking that weakened the corners of the specimen.
6. The comparison with a Critical Shear Crack Theory based model for the prediction of the capacity of the specimens indicates that the model is adequate in predicting the overall behavior and failure modes. The model shows that even a small zone with HPFRC has the potential of avoiding punching and promoting a flexural/flexure induced failure. The model predicts a significant capacity increase due to HPFRC. Further research is recommended to assess the ultimate punching capacity of flat slabs with HPFRC failing within the HPFRC zone.

CRediT authorship contribution statement

Brisid Isufi: Conceptualization, Methodology, Formal analysis, Investigation, Data curation, Writing – original draft, Writing – review & editing, Visualization. **João Pedro Relvas:** Formal analysis, Investigation, Data curation. **Carla Marchão:** Conceptualization, Methodology, Formal analysis, Investigation, Writing – review & editing, Supervision. **António Pinho Ramos:** Conceptualization, Methodology, Writing – review & editing, Resources, Supervision.

Declaration of Competing Interest

The authors declare that they have no known competing financial interests or personal relationships that could have appeared to influence the work reported in this paper.

Acknowledgements

This work was financially supported by the Fundação para a Ciência e Tecnologia – Ministério da Ciência, Tecnologia e Ensino Superior through project PTDC/ECI-EST/ 30511/2017 funded by national funds (PIDDAC). EUROMODAL, Secil, Omya Comital, Sika and Dramix are gratefully acknowledged for their collaboration and supply of materials.

References

[1] Swamy RN, Ali SAR. Punching Shear Behavior of Reinforced Slab-Column Connections Made with Steel Fiber Concrete. ACI J Proc 1982;79. https://doi.org/10.14359/10917.
[2] Narayanan R, Darwish IYS. Punching shear tests on steel-fibre-reinforced micro-concrete slabs. Mag Concr Res 1987;39(138):42–50. https://doi.org/10.1680/macr.1987.39.138.42.
[3] Marzouk H, Hussein A. Experimental investigation on the behaviour of high-strength concrete slabs. ACI Struct J 1991:701–13. https://doi.org/10.14359/1261.
[4] Isufi B, Pinho RA. A review of tests on slab-column connections with advanced concrete materials. Structures 2021;32:849–60. https://doi.org/10.1016/j.istruc.2021.03.036.
[5] Chanthabouala K, Teng S, Chandra J, Tan K-H, Ostertag CP. Punching Tests of Double-Hooked-End Fiber Reinforced Concrete Slabs. ACI Struct J 2018;115. doi: 10.14359/51706891.
[6] Ozden S, Ersoy U, Ozturan T. Punching shear tests of normal- and high-strength concrete flat plates. Can J Civ Eng 2006;33(11):1389–400. https://doi.org/10.1139/l06-089.
[7] Qi J, Cheng Z, Zhou K, Zhu Y, Wang J, Bao Yi. Experimental and theoretical investigations of UHPC-NC composite slabs subjected to punching shear-flexural failure. J Build Eng 2021;44:102662. https://doi.org/10.1016/j.jobe.2021.102662.
[8] Inácio MMG, Lapi M, Pinho Ramos A. Punching of reinforced concrete flat slabs – Rational use of high strength concrete. Eng Struct 2020;206:110194. https://doi.org/10.1016/j.engstruct.2020.110194.
[9] Hallgren M. Punching Shear Capacity of Reinforced High Strength Concrete Slabs. KTH Royal Institute of Technology 1996.
[10] Gouveia ND, Faria DMV, Ramos AP. Assessment of SFRC flat slab punching behaviour – part I: monotonic vertical loading. Mag Concr Res 2019;71(11):587–98. https://doi.org/10.1680/jmacr.17.00343.
[11] McHarg PJ, Cook WD, Mitchell D, Yoon Y. Benefits of Concentrated Slab Reinforcement and Steel Fibers on Performance of Slab-Column Connections. ACI Struct J 2000;97:225–35.
[12] Cheng M-Y, Parra-Montesinos GJ. Evaluation of Steel Fiber Reinforcement for Punching Shear Resistance in Slab-Column Connections - Part I: Monotonically Increased Load. ACI Struct J 2010;107:101–9. https://doi.org/10.14359/51663394.
[13] Zohrevand P, Yang X, Jiao X, Mirmiran A. Punching Shear Enhancement of Flat Slabs with Partial Use of Ultrahigh-Performance Concrete. J Mater Civ Eng 2015;27(9):04014255.
[14] Nunes S, Pimentel M, Sousa C. Mechanical and fracture behaviour of an hpfrc. BEfib2021. Valencia: RILEM-fib; 2021.
[15] Blazy J, Nunes S, Sousa C, Pimentel M. Development of an HPFRC for Use in Flat Slabs. RILEM Bookseries 2021;30:209–20. https://doi.org/10.1007/978-3-030-58482-5_19.
[16] CEN. EN 1992-1-1. Eurocode 2 — Design of concrete structures. Part 1-1: General rules and rules for buildings. 2004.
[17] CEN. EN 12350-8. Testing Fresh Concrete, Part 8: Self-Compacting Concrete—Slump–Flow Test. 2010.
[18] CEN. EN 12390-3. Testing Hardened Concrete Part 3: Compressive Strength of Test Specimens. 2019.
[19] CEN. EN 12390-13. Testing hardened concrete , Part 13: Determination of secant modulus of elasticity in compression. 2013.
[20] CEN. EN 12390-6. Testing hardened Concrete Part 6: Tensile Splitting Strength of Test Specimens. 2000.
[21] Koppitz R, Kenel A, Keller T. Effect of load history on punching shear resistance of flat slabs. Eng Struct 2015;90:130–42. https://doi.org/10.1016/j.engstruct.2015.02.016.
[22] Maya LF, Fernández Ruiz M, Muttoni A, Foster SJ. Punching shear strength of steel fibre reinforced concrete slabs. Eng Struct 2012;40:83–94. https://doi.org/10.1016/j.engstruct.2012.02.009.
[23] Harajli MH, Maalouf D, Khatib H. Effect of fibers on the punching shear strength of slab-column connections. Cem Concr Compos 1995;17(2):161–70. https://doi.org/10.1016/0958-9465(94)00031-S.
[24] de Sousa AMD, Lantsoght EOL, Genikomsou AS, Krahl PA, El Debs MK. Behavior and punching capacity of flat slabs with the rational use of UHPFRC: NLFEA and analytical predictions. Eng Struct 2021;244:112774. https://doi.org/10.1016/j.engstruct.2021.112774.
[25] Muttoni A. Punching Shear Strength of Reinforced Concrete Slabs. ACI Structral J 2008;105:440–50. https://doi.org/10.14359/19858.
[26] fib. fib Model Code for Concrete Structures 2010. Weinheim, Germany: Wiley-VCH Verlag GmbH & Co. KGaA; 2013. doi:10.1002/9783433604090.
[27] Ramos A, Isufi B. HiPerSlab - Enhancement of the Structural Behaviour of Flat Slabs under Cyclic and Seismic Actions through the Rational Use of High Performance Fibre Reinforced Concrete, Final Report, Project PTDC/ECI-EST/30511/2017. Lisbon: 2022.